ACS OMEGA

Open Access



http://pubs.acs.org/journal/acsodf

Article

# Systematic Analysis of Disulfidptosis-Related lncRNAs in Hepatocellular Carcinoma with Vascular Invasion Revealed That AC131009.1 Can Promote HCC Invasion and Metastasis through Epithelial−Mesenchymal Transition

Xuefeng Gu, Yanyan Wei, Mao Lu, Duo Shen, Xin Wu, and Jin Huang*

Cite This: *ACS Omega* 2024, 9, 49986−49999

Read Online

ACCESS | Metrics & More | Article Recommendations | Supporting Information

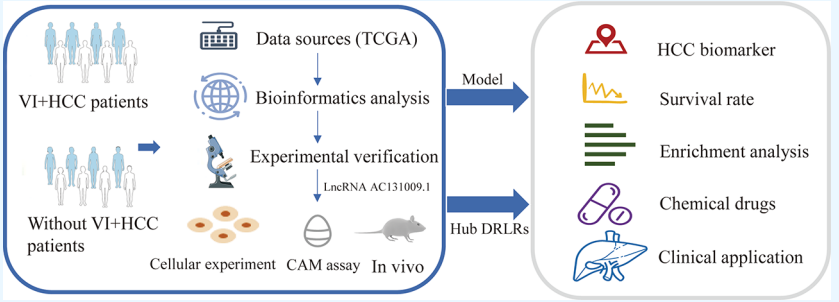


**ABSTRACT:** Disulfidptosis, a recently identified pathway of cellular demise, served as the focal point of this research, aiming to pinpoint relevant lncRNAs that differentiate between hepatocellular carcinoma (HCC) with and without vascular invasion while also forecasting survival rates and responses to immunotherapy in patients with vascular invasion (VI+). First, we identified 300 DRLRs in the TCGA database. Subsequently, utilizing univariate analysis, LASSO-Cox proportional hazards modeling, and multivariate analytical approaches, we selected three DRLRs (AC009779.2, AC131009.1, and LUCAT1) with the highest prognostic value to construct a prognostic risk model for VI+ HCC patients. Multivariate Cox regression analysis revealed that this model is an independent prognostic factor for predicting overall survival that outperforms traditional clinicopathological factors. Pathway analysis demonstrated the enrichment of tumor and immune-related pathways in the high-risk group. Immune landscape analysis revealed that immune cell infiltration degrees and immune functions had significant differences. Additionally, we identified valuable chemical drugs (AZD4547, BMS-536924, BPD-00008900, dasatinib, and YK-4-279) for high-risk VI+ HCC patients. In-depth bioinformatics analysis was subsequently conducted to assess immune characteristics, drug susceptibility, and potential biological pathways involving the three hub DRLRs. Furthermore, the abnormally elevated transcriptional levels of the three DRLRs in HCC cell lines were validated through qRT-PCR. Functional cell assays revealed that silencing the expression of lncRNA AC131009.1 can inhibit the migratory and invasive capabilities of HCC cells, a finding further corroborated by the chorioallantoic membrane (CAM) assay. Immunohistochemical analysis and hematoxylin−eosin staining (HE) staining provided preliminary evidence that AC131009.1 may promote the invasion and metastasis of HCC cells by inducing epithelial−mesenchymal transition (EMT) in both subcutaneous xenograft models and orthotopic HCC models within nude mice. To summarize, we developed a risk assessment model founded on DRLRs and explored the potential mechanisms by which hub DRLRs promote HCC invasion and metastasis.

## 1. INTRODUCTION

In 2020, hepatocellular carcinoma (HCC) ranked sixth in terms of incidence and the third leading cause of death among the top ten most common cancers.[1] Projections suggest that by 2025, the incidence of HCC may rise to one million cases.[2] There are many treatment modalities for HCC including surgical interventions, techniques for ablation, radioembolization via transarterial routes, chemoembolization administered transarterially, and systemic treatment approaches.[3]

Additionally, advancements in molecular targeted therapies and immunotherapies are showing significant promise in the management of HCC.[4−7] However, despite these advancements, the prognosis for HCC patients remains poor, with a 5-year relative survival rate of only 20%.[8]

Vascular invasion (VI) is characterized by the infiltration of neoplastic cells into the branches of the portal vein or hepatic

Received: October 15, 2024
Revised: November 14, 2024
Accepted: November 19, 2024
Published: December 3, 2024





https://doi.org/10.1021/acsomega.4c09411
*ACS Omega* 2024, 9, 49986−49999

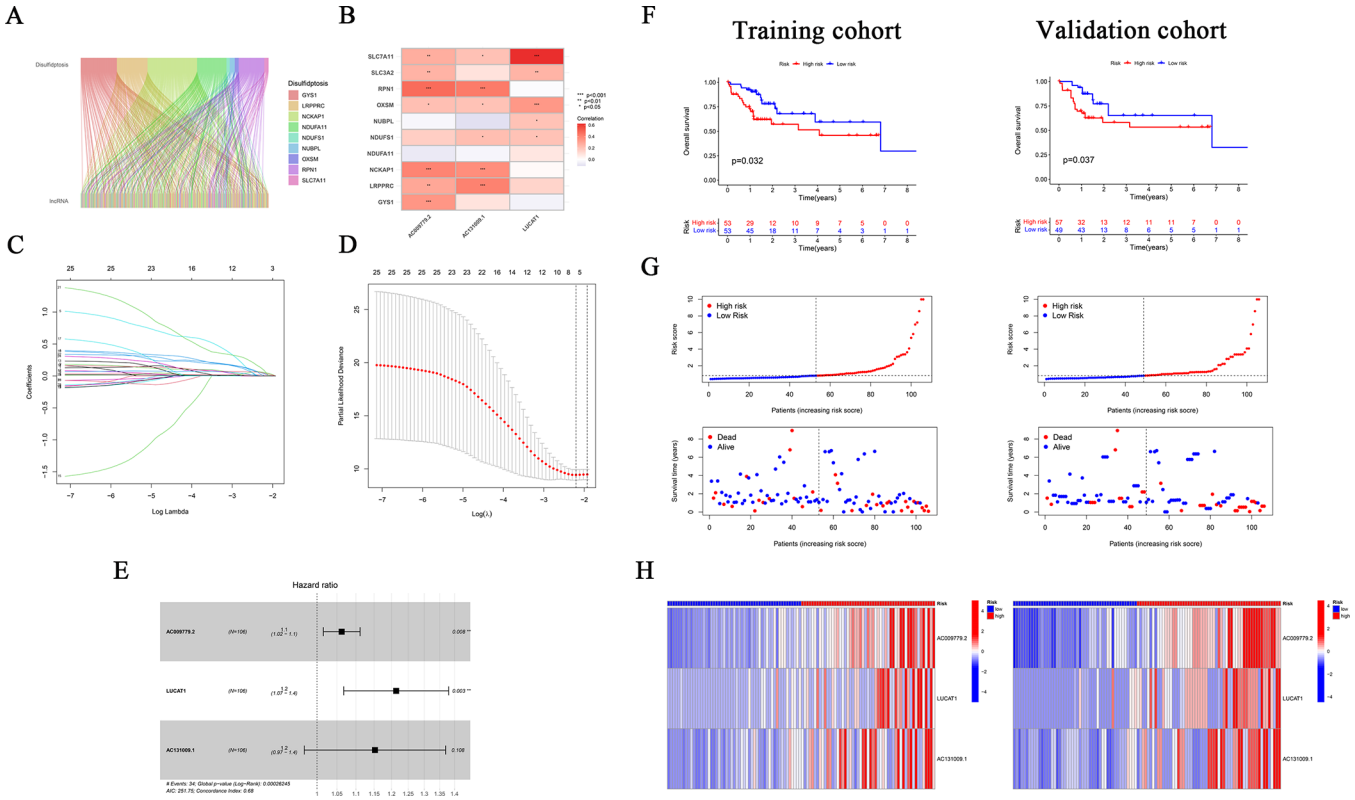


**Figure 1.** Construction of the prognostic disulfidptosis-related lncRNA (DRLR) risk model for hepatocellular carcinoma (HCC).} (A) Sankey diagram showing the coexpression patterns of disulfidptosis-associated genes with DRLRs in VI HCC. (B) coexpression between 10 disulfidptosis-related genes and three prognostic lncRNAs independent of disulfidptosis. (C, D) Prognostic prediction model using the least absolute shrinkage and selection operator (LASSO)-Cox regression analysis. (E) Multivariable Cox regression analysis determined 3 hub DRLRs. (F) Kaplan−Meier survival curves for risk cohorts in both validation and training data sets. (G) distribution of risk scores and survival status within HCC cohorts. (H) Heatmap representing the expression of the three prognostic DRLRs in the examined cohorts.

vein within the liver. An increasing body of literature indicates that VI serves as a negative prognostic marker in HCC.[9−11]

Clinicians can make informed decisions regarding appropriate surgical strategies for patients by considering the presence of preoperative VI. In recent years, researchers have been investigating the risk and prognostic factors associated with intrahepatic vascular invasion (IVI) in HCC. Zeng et al.[12] developed a nomogram utilizing the SEER database to predict VI in HCC patients, providing valuable guidance for clinical decision-making. Peng et al.[13] constructed a nomogram utilizing radiomic characteristics, which exhibited high predictive accuracy for VI status in HBV-related HCC patients. Furthermore, Wang et al.[14] highlighted that both the maximum microvascular invasion (MVI) stage and its corresponding area could serve as independent prognostic indicators, effectively forecasting long-term overall survival rates in individuals exhibiting MVI post-R0 hepatic resection. Consequently, it is essential to investigate specific genetic biomarkers that can aid in the identification of vascular invasive behavior and the prognosis of HCC.

Liu et al.[15] recently identified disulfidptosis as a novel cell death form, distinct from other programmed cell death processes, characterized by Rac-WRC promoted actin polymerization and lamellipodia formation. In SLC7A11-overexpressing cells exposed to glucose deprivation, cystine intake rises, causing NADPH depletion, which disrupts normal disulfide bonding in actin cytoskeleton proteins, leading to network collapse and cell death.

Additionally, the researchers observed that supplying additional cystine to glucose-starved, SLC7A11-deficient 786-O cells reduces cellular NADPH levels, induces actin protein disulfide bonding and F-actin contraction, and triggers robust cell death. This discovery of disulfidptosis opens avenues for developing novel therapeutic strategies and identifying potential disease targets.

Long noncoding RNAs (lncRNAs) are RNA molecules primarily found in the cell nucleus or cytoplasm.[16] They have a length exceeding 200 nucleotides and do not possess the ability to encode proteins. Extensive research has demonstrated the substantial involvement of lncRNAs in the initiation and progression of HCC, making them valuable prognostic markers.[17−19]

Although the role of disulfidptosis and related lncRNAs in HCC remains ambiguous, the pathways contributing to HCC invasion and metastasis are yet to be fully understood. There is also a lack of predictive models developed for disulfidptosis-related lncRNAs (DRLRs) in tumor development. In particular, disulfidptosis and DRLRs may play a more significant role in HCC patients with VI than in those without VI. However, the mechanisms by which they promote HCC invasion and metastasis remain to be explored. Therefore, in the context of our research, we aimed to establish a predictive characteristic framework utilizing DRLRs to distinguish HCC patients with VI from those without VI utilizing the Cancer Genome Atlas (TCGA) database. Furthermore, we conducted comprehensive comparative analyses of the immune status,


https://doi.org/10.1021/acsomega.4c09411
ACS Omega 2024, 9, 49986−49999

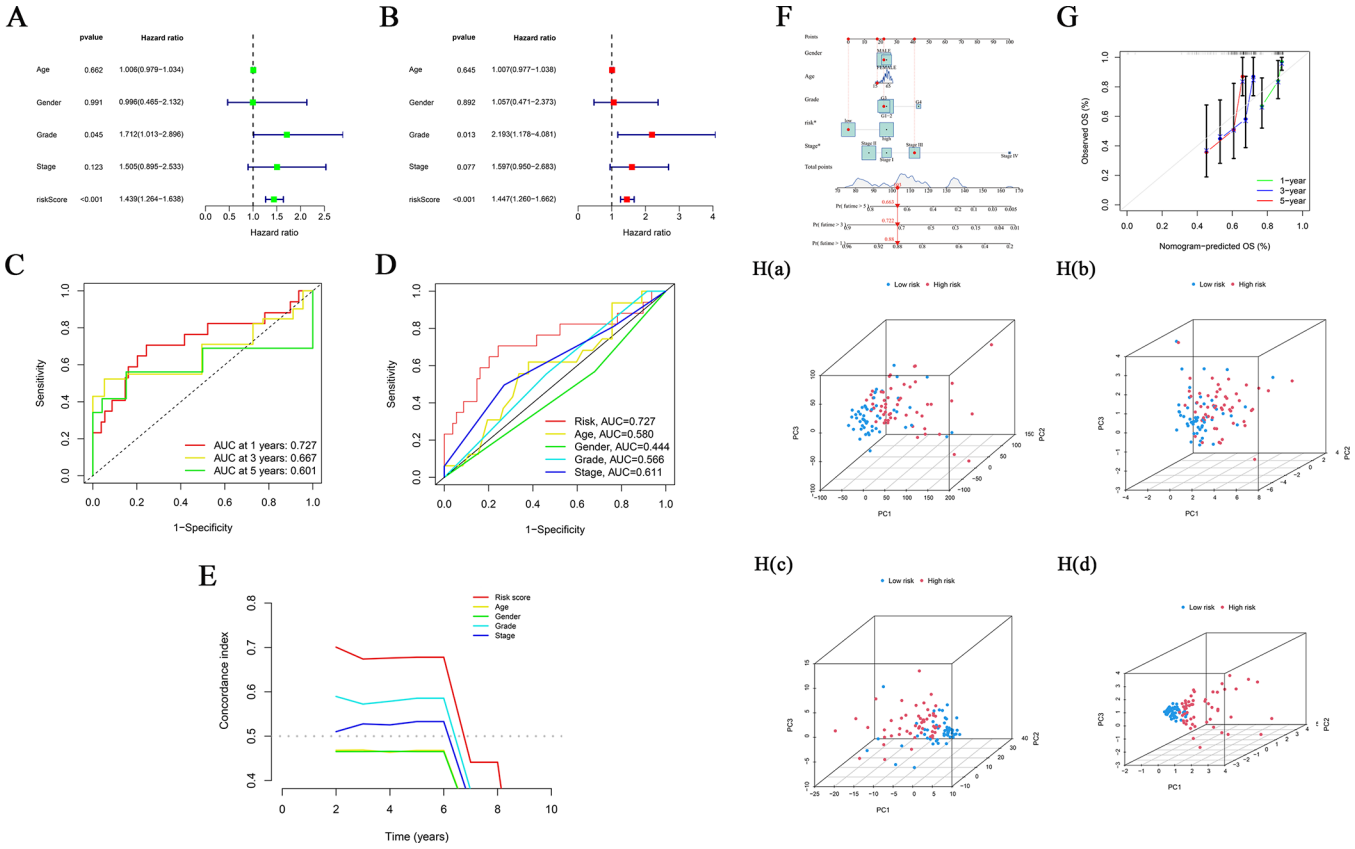


**Figure 2.** Independent prognostic factor analysis based on VI+ HCC patient overall survival (OS).} (A) In the univariate Cox analysis, notable differences were observed in pathological characteristics and risk scores, which were statistically significant. (B) Multivariate Cox analysis also revealed significant statistical disparities in pathological characteristics and risk computations. (C) The time receiver operating characteristic (timeROC) curve predicts the 1-, 3-, and 5-year OS among patients with VI+ HCC. (D) The MultiROC assessment demonstrated that the predictive accuracy of the proposed risk model surpasses other clinical parameters. (E) According to the C-index, the prognostic precision of the risk model outperforms other clinical measures. (F) A nomogram constructed from the 3-DRLR signature score provides a prognostic prediction. (G) The calibration curve assists in forecasting overall survival (OS) at 1-year, 3-year, and 5-years. (H) Principal component analysis (PCA) was conducted to differentiate between high-risk and low-risk groupings across (Ia) all genes, (Ib) disulfidoptosis-related genes, (Ic) DRLRs, and (Id) prognostic markers associated with 3-DRLRs.

gene set enrichment, tumor microenvironment features, and chemotherapy drug response among different risk groups. Additionally, we experimentally validated the expression of three independent prognostic DRLRs at the cellular level. Finally, functional validation of the prognostic lncRNA AC131009.1 in HCC was performed through knockdown experiments. Preliminary findings suggest that AC131009.1 may promote the spread and metastatic progression of HCC by triggering epithelial-mesenchymal transition (EMT), thus providing a potential target for HCC treatment. In conclusion, our study provides an effective prognostic model based on DRLRs and offers preliminary insights into the potential mechanisms by which AC131009.1 promotes HCC invasion and metastasis. These findings have the potential to facilitate personalized treatment for individuals diagnosed with HCC.

## 2. RESULTS

**2.1. Identification of Hub DRLRs and Construction of the DRLR-Based Model.** After the initial screening, a total of 300 lncRNAs were found to have coexpression relationships with disulfidptosis-related genes (Figure 1A). An initial univariate Cox regression analysis uncovered 25 DRLRs. These 25 lncRNAs were further selected using least absolute shrinkage and selection operator (LASSO) regression, leading to the identification of 5 DRLRs: AC009779.2, AC131009.1, LUCAT1, AL359313.1, and AC011416.3 (Figure 1C and D).

Subsequently, a multivariate Cox regression analysis was conducted to establish a risk model, ultimately identifying 3 DRLRs for inclusion: AC009779.2, AC131009.1, and LUCAT1 (Figure 1E). The risk score formula was calculated using the coefficients of these DRLRs: Risk Score = (0.06049 × AC009779.2 expression) + (0.14195 × AC131009.1 expression) + (0.19371 × LUCAT1 expression). Figure 1B displays the correlation heatmap between the 3 selected hub DRLRs and disulfidptosis-related genes. Following a resampling procedure with replacement, the clinical data from both the internal validation cohort and the training cohort exhibited comparability in terms of their clinical features ($P > 0.05$, Table S1). In the training data set, patients were stratified into high-risk and low-risk categories according to the median value of their risk scores. Kaplan−Meier survival analysis indicated a worse prognosis for VI+ HCC patients in the high-risk category compared to the low-risk group, both in training and validation data sets (Figure 1F). Figure 1G illustrates the risk score distribution and survival outcome, highlighting the increased mortality rate among high-risk VI+ HCC patients. The heatmap represents the expression levels of the three hub DRLRs in both the testing and training cohorts (Figure 1H).


https://doi.org/10.1021/acsomega.4c09411
ACS Omega 2024, 9, 49986−49999

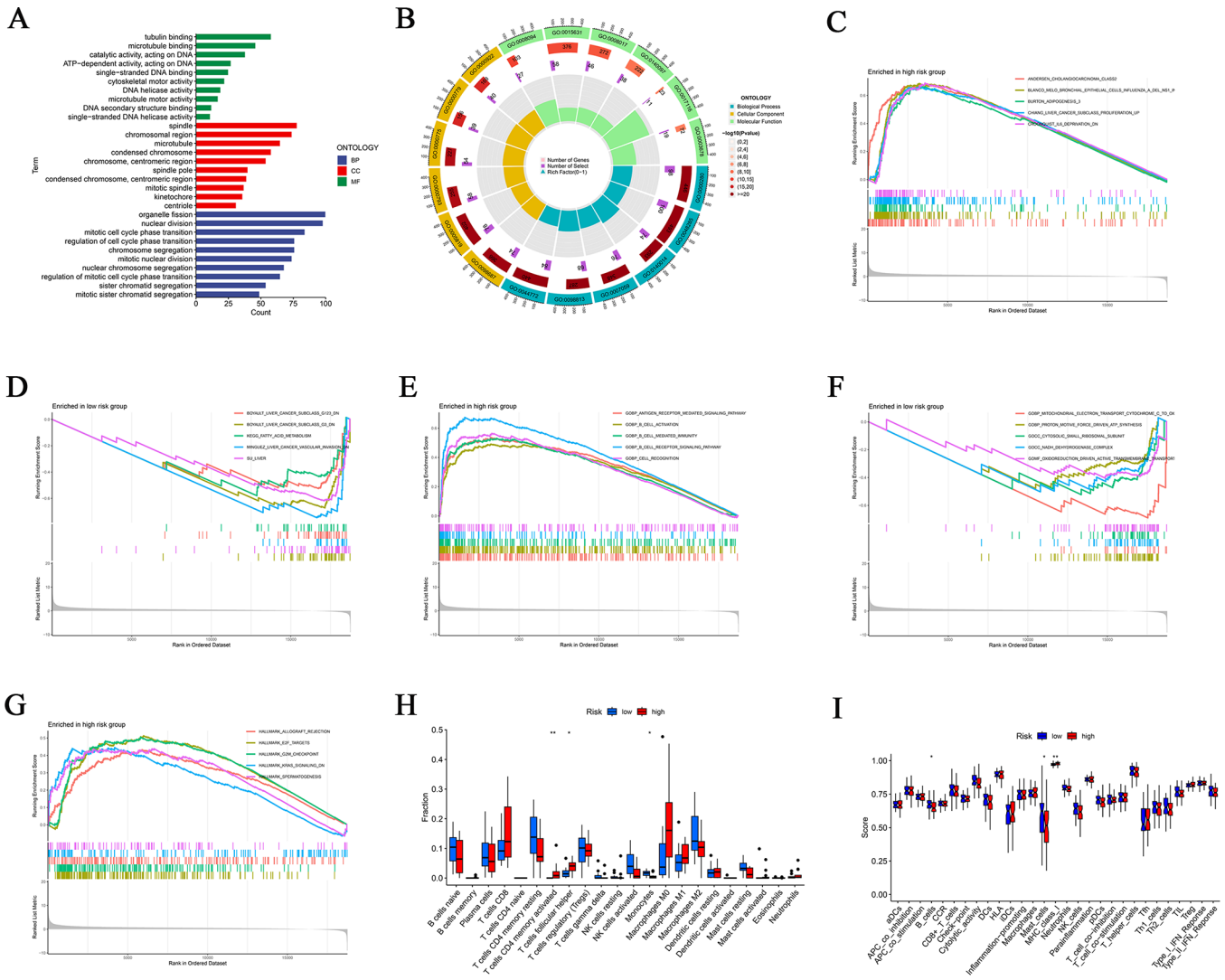


**Figure 3.** Elucidates the outcomes of Gene Ontology (GO) and Gene Set Enrichment Analysis (GSEA). (A) Displaying a bar chart representing the ten GO terms with the highest significance in enrichment. (B) Showing a circle diagram derived from GO enrichment analysis results. GSEA showed substantial discrepancies in the enrichment of the TCGA VI+ HCC cohort for the c2.all.v2022.1.Hs.symbols.gmt gene set between high-risk (C) and low-risk cohorts (D), as determined by the 3-DRLR signature. Similarly, the c5.all.v2022.1.Hs.symbols.gmt gene set showed differences between the high-risk (E) and low-risk cohorts (F). (G) Highlights significant enrichment of the h.all.v2022.1.Hs.symbols.gmt gene set in the high-risk cohort. (H) presents the percentages of 22 immune cell types in both the high- and low-risk groups as computed by the CIBERSORT methodology. (I) Comparison of immune function scores between patients categorized into low-risk and high-risk cohorts.

**2.2. The Prognostic Significance of the Risk Score as an Independent Factor.** In terms of the prognostic significance of the risk score as an independent factor, Figures 2A and 2B indicate that the risk score yielded p-values below 0.001, highlighting its potential as a standalone prognostic marker for patients with VI+ HCC. The area under the curve (AUC) for predicting survival outcomes at 1, 3, and 5 years were 0.727, 0.667, and 0.601, respectively (Figure 2C). These findings indicate that our 3-DRLR model exhibited the best short-term prognostic predictive efficacy for VI+ HCC patients at 1 year. Furthermore, the multi-receiver operating characteristic (ROC) curve in Figure 2D demonstrated that the risk score's AUC of 0.727 surpassed those of clinical factors such as age, sex, pathological characteristics, and TNM stage, indicating its superior capability in prognosticating overall survival for VI+ HCC patients. The C-index analysis corroborated the superior predictive accuracy of the risk score compared to the stated clinical features (Figure 2E). A prognostic nomogram was developed using the patient risk score, along with sex, age, TNM tumor stage, and pathological characteristics. As shown in Figure 2F, for the 20th patient, the score was calculated at 103. The AUCs of this model for estimating survival probabilities at 1, 3, and 5 years were 0.880, 0.722, and 0.663, respectively. Furthermore, the calibration curve in Figure 2G demonstrated strong concordance between the predicted outcomes generated by the model and the actual results that were observed. Principal Component Analysis (PCA) was conducted to explore the expression profiles concerning all genes (Figure 2Ha), disulfidptosis-related genes (Figure 2Hb), and DRLRs (Figure 2Hc). However, these analyses proved inadequate in effectively distinguishing high-risk cohorts from low-risk ones. Conversely, the key DRLRs identified in the 3-DRLR model demonstrated a superior capability to differentiate between high-risk and low-risk groups among patients with vascular invasion-positive hepatocellular carcinoma (VI+ HCC) (Figure 2Hd).



https://doi.org/10.1021/acsomega.4c09411
ACS Omega 2024, 9, 49986−49999

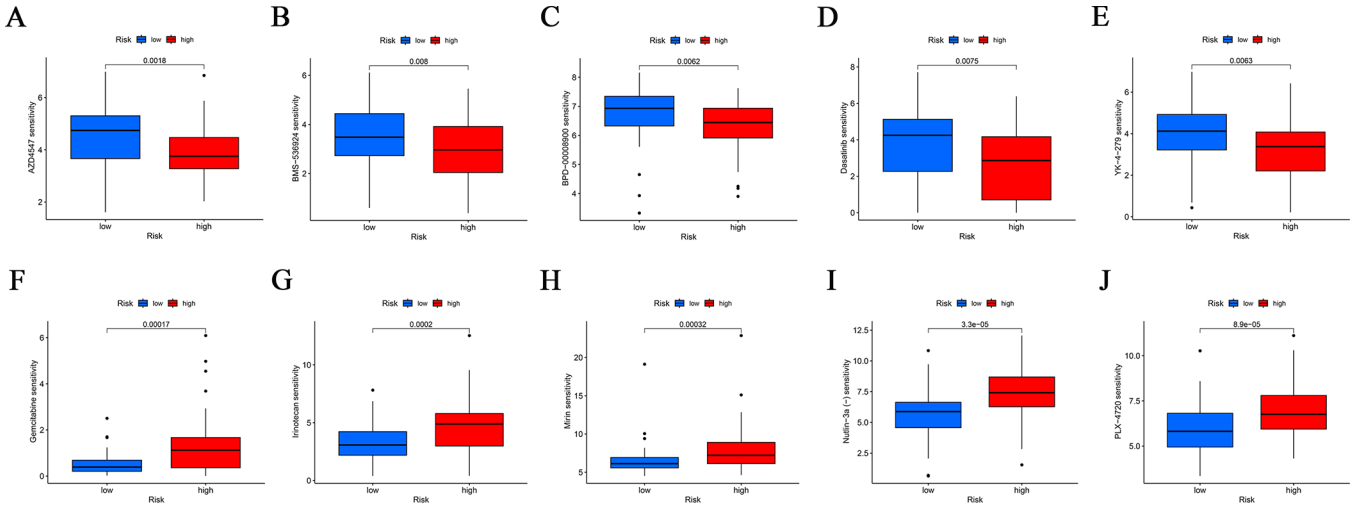


**Figure 4.** Drug sensitivity profiles for VI+ HCC patients in high-risk and low-risk groups based on the 3-DRLR signature. Analysis of the distribution of the half maximal inhibitory concentration (IC50) revealed significant differences between patients in the high-risk group and low-risk group for (A) AZD4547, (B) BMS-536924, (C) BPD-00008900, (D) dasatinib, (E) YK-4−279, (F) gemcitabine, (G) irinotecan, (H) mirin, (I) Nutlin-3a (−), and (J) PLX-4720.

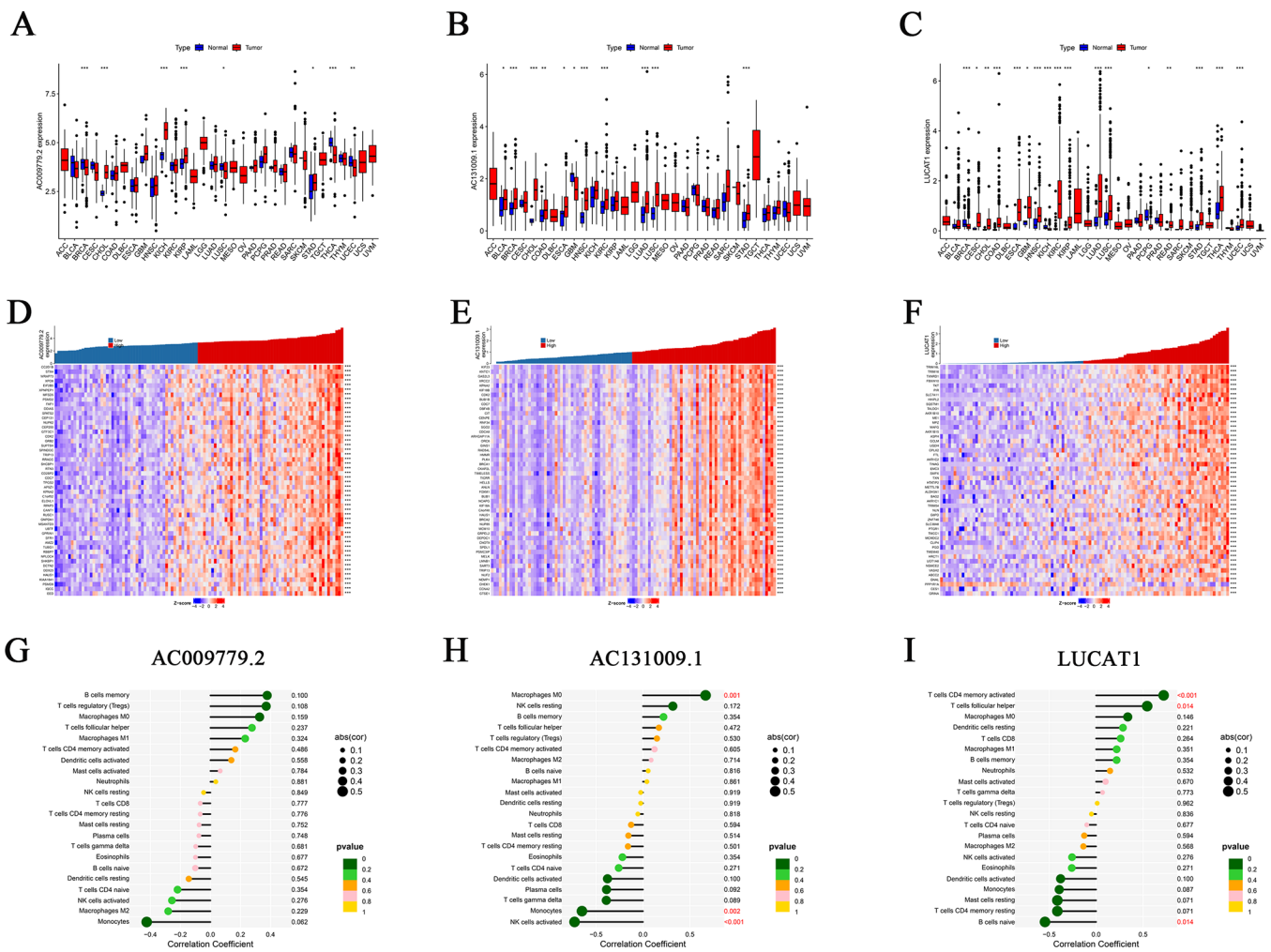


**Figure 5.** Risk hub prognostic lncRNAs analysis in the 3-DRLR signature. Pancancer analysis showed differential expression of AC009779.2 (A), AC131009.1 (B), and LUCAT1 (C) in tumor and paracancerous tissues. Coexpression of the top 50 genes and 3 disulfidptosis-independent prognostic hub lncRNAs. The correlation heatmap shows the top 50 gene significantly coexpressed with AC009779.2 (D), AC131009.1 (E), and LUCAT1 (F). The relationship between the relative quantities of 22 immune cell types and the expression levels of lncRNA AC009779.2 (G), AC131009.1 (H), and LUCAT1 (I).



https://doi.org/10.1021/acsomega.4c09411
ACS Omega 2024, 9, 49986−49999

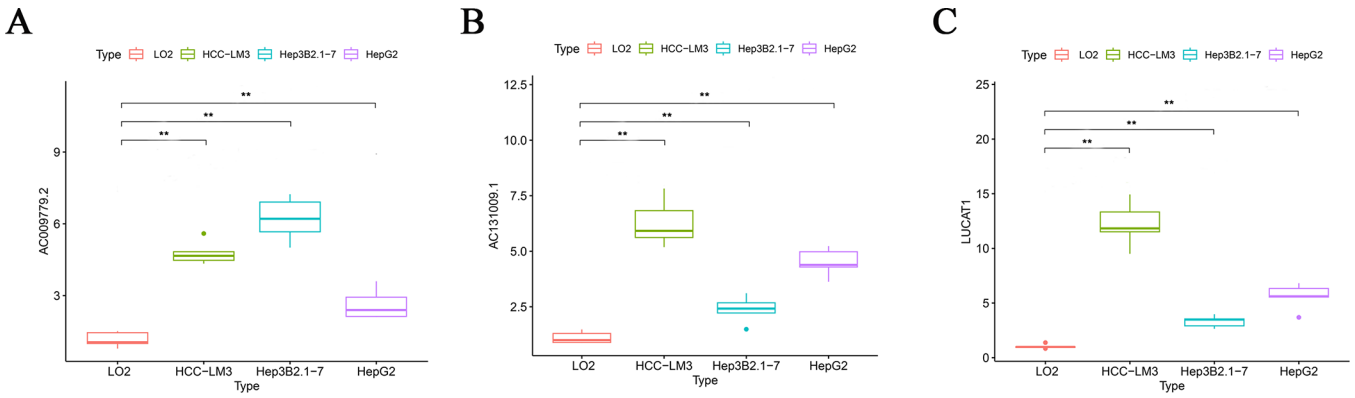


**Figure 6.** Validation of expression levels for prognostic hub lncRNAs within the context of the 3-DRLR model across different HCC cell lines. Expression levels of AC009779.2 (A), AC131009.1 (B), and LUCAT1 (C) were determined in HCC-LM3, Hep3B2.1−7, and HepG2 cell lines and contrasted against the normal liver cell line, L02. Data are presented as the mean ± standard deviation (SD) with $n = 5$. Statistically significant differences are indicated by **P < 0.01.

**2.3. Gene Ontology (GO) Pathway Enrichment Study and Gene Set Enrichment Analysis (GSEA).** A comprehensive analysis identified a total of 1,637 genes exhibiting differential expression when comparing groups at high risk with those at low risk. Findings from the GO enrichment analysis (Figure 3A and B) reveal that these DEGs are largely linked with biological processes such as mitotic nuclear division, organelle fission, nuclear division, chromosome segregation, and nuclear chromosome segregation. Principal cellular components enriched include regions of chromosomes, the spindle apparatus, compacted chromosomes, centromeric regions of chromosomes, and centromeres of condensed chromosomes. Enriched molecular functions primarily relate to ATPase activity on DNA, tubulin and microtubule binding, DNA catalytic activity, and single-stranded helicase pathways. Gene Set Enrichment Analysis (GSEA) of the risk cohorts demonstrated that within the c2.all.v2022.1.Hs.symbols.gmt gene set, pathways including andersen cholangiocarcinoma class2, blanco melo bronchial epithelial cells influenza a del ns1 infection dn, and burton adipogenesis 3 show notable activation in the high-risk cohort (Figure 3C). On the contrary, the low-risk cohort is significantly enriched in pathways such as boyault liver cancer subclass g123 dn, boyault liver cancer subclass g3 dn, and kegg fatty acid metabolism (Figure 3D). In the context of the c5.all.v2022.1.Hs.symbols.gmt data set, high-risk patients are involved in cellular pathways and immune responses, including antigen receptor-mediated signaling, B cell-mediated immunity, and B cell activation (Figure 3E). Meanwhile, the low-risk cohort's pathways comprise mitochondrial electron transport from cytochrome c to oxygen, ATP production driven by proton motive force, and the cytosolic small ribosomal subunit (Figure 3F). Regarding the h.all.v2022.1.Hs.symbols.gmt set, high-risk patients primarily participated in pathways like hallmark allograft rejection, hallmark E2F targets, and hallmark G2M checkpoint (Figure 3G). Notably, there was no significant enrichment observed with in the low-risk cohort.

**2.4. Exploration of the Immune Landscape in VI+ HCC Patients Based on the 3-DRLR Model.** The examination of immune infiltration via the CIBERSORT platform and the single sample gene set enrichment analysis (ssGSEA) methodology divulged a notably elevated presence of follicular helper T cells and activated memory CD4 T cells within the high-risk cohort in comparison to the low-risk cohort. Conversely, monocytes were found to be markedly more prevalent in the low-risk cohort than their high-risk counterparts (Figure 3H). The immune function scoring results indicated that B cells and mast cells were significantly less abundant in the high-risk cohort, whereas immune-related MHC class I molecules were more pronounced in this group (Figure 3I). These observations suggest that the prognostic risk score based on DRLRs proficiently mirrors the immunological landscape of VI+ HCC patients, offering critical insights for predicting both the response to immunotherapy and the prognosis for VI+ HCC patients.

**2.5. Drug Sensitivity Analysis of VI+ HCC Based on the 3-DRLR Model.** To explore potential chemotherapeutic and targeted drugs that may exhibit sensitivity in VI+ HCC patients in the high-risk cohort, this study conducted drug sensitivity analysis using oncoPredict to determine the IC50 concentrations of various drugs. The findings revealed that AZD4547, BMS-536924, BPD-00008900, dasatinib, and YK-4−279 were the five most sensitively responded drugs within the high-risk patient cohort (Figure 4A-E). Conversely, the drugs that exhibited the greatest resistance in this group included gemcitabine, irinotecan, mirin, nutlin-3a (−), and PLX-4720 (Figure 4F-J). Our study provides valuable references for clinical drug selection.

**2.6. Bioinformatics Examination of Prognostic Hub DRLRs within the Framework.** We further conducted a pancancer analysis (including 32 other cancer types as documented within the TCGA repository) to examine the differential expression patterns of the three hub lncRNAs identified in our study. The pan-cancer analysis revealed differential expression of three hub lncRNAs, AC009779.2, AC131009.1, and LUCAT1 in different tumors (Figures 5A-C). To gain insights into the genes potentially regulated by these three high-risk hub lncRNAs, we performed coexpression analysis to identify genes coexpressed with these three lncRNAs. The correlation heatmaps of the top 50 genes are presented in Figure 5D-F. Additionally, we conducted GO analyses and GSEA to explore the biological pathways linked to these three high-risk hub lncRNAs, and the results are presented in Figure S1-3. Furthermore, we employed the Spearman method to further investigate the correlations between the three prognostic hub DRLRs and the infiltration levels of 22 immune cells. The results revealed that, except for AC009779.2 levels (Figure 5G), AC131009.1 (Figure 5H) and


https://doi.org/10.1021/acsomega.4c09411
ACS Omega 2024, 9, 49986−49999

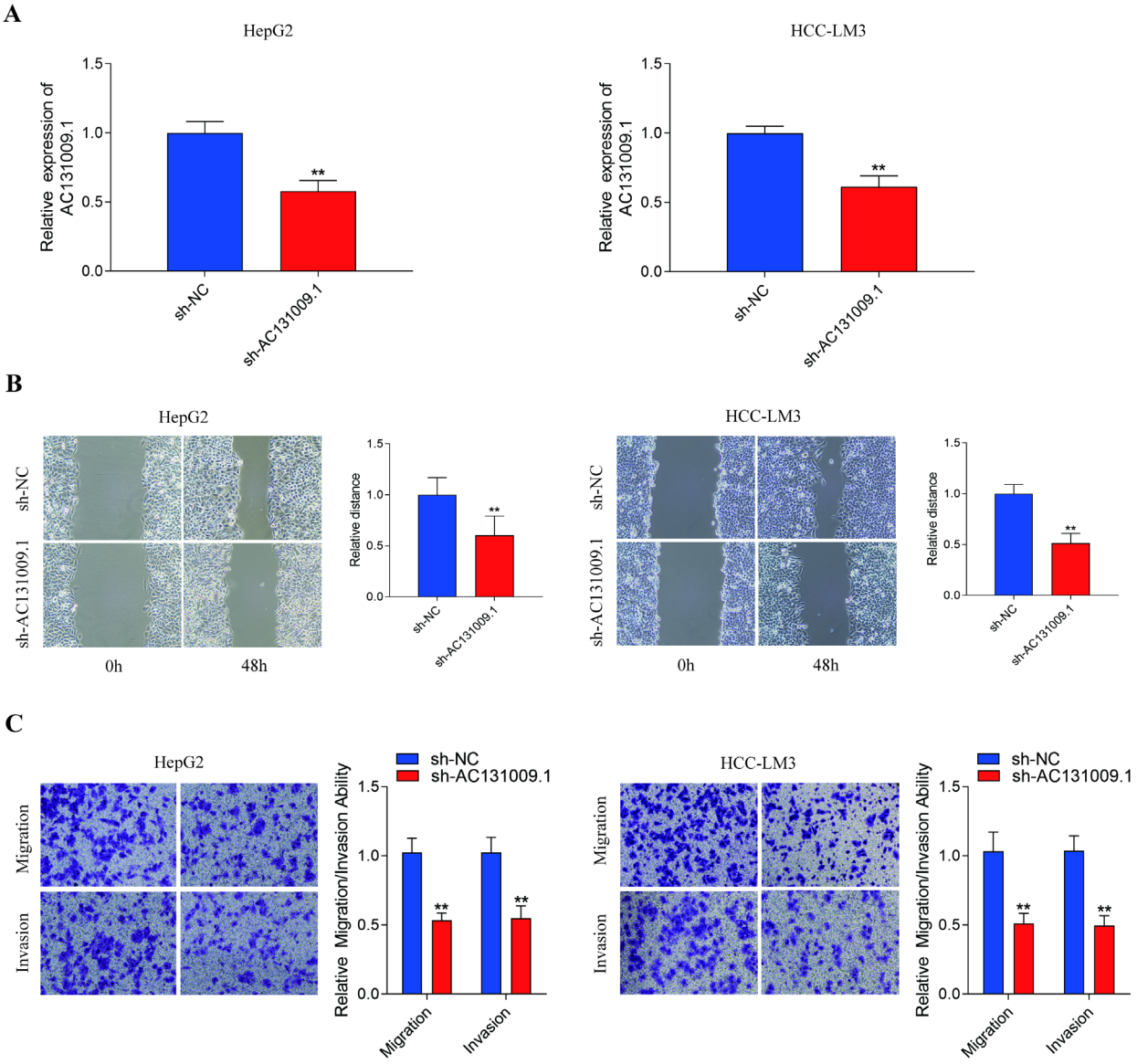


**Figure 7.** Impacts of lncRNA AC131009.1 on HCC cell migration and invasion. (A) The knockdown efficiency of sh-AC131009.1 compared with the negative control (NC) in HCC-LM3 and HepG2 cells was measured by qRT-PCR. (B) Wound healing assays of HepG2 and HCC-LM3 cells transfected with sh-AC131009.1 and sh-NC. (C) Transwell assays of HepG2 and HCC-LM3 cells transfected with sh-NC and sh-AC131009.1. Data are presented as mean ± SD ($n$ = 3). Significant differences are denoted by **P < 0.01.

LUCAT1 (Figure 5I) levels exhibited significant correlations with the levels of different types of immune cells. Specifically, AC131009.1 levels correlated positively with M0 macrophages (P = 0.001) and negatively with both monocytes (P = 0.002) and activated NK cells (P < 0.001). For LUCAT1, a significant positive correlation was identified with follicular helper T cells (P = 0.014) and activated memory CD4 T cells (P < 0.001), whereas naive B cells were negatively correlated (P = 0.014). Finally, we presented patients' drug sensitivity in relation to the expression profiles of the three hub lncRNAs (Figures S4−6).

**2.7. Elucidating the Expression Levels of the Prognostic Hub DRLRs within HCC Cell Lines through the Application of Quantitative Real-Time PCR (qRT-PCR).** Furthermore, we explored the expression levels of the prognostic hub DRLRs within HCC cell lines using quantitative real-time PCR (qRT-PCR). Our analysis, illustrated in Figure 6, demonstrated a notable upregulation of the three hub DRLRs in HCC cell lines when compared to the normal liver cell line, L02. This observation suggests a crucial role for these hub DRLRs in HCC pathology. Specifically, in the highly metastatic HCC-LM3 cell line, the expression levels of AC131009.1 and LUCAT1 were significantly higher than those observed in the less invasive cell lines, Hep3B2.1−7 and HepG2. Despite the limited existing literature on the role of AC131009.1 in HCC, to enhance our understanding of the influence of DRLRs on the invasive and metastatic characteristics of HCC cells, we selected AC131009.1 for subsequent cellular functional experiments and conducted preliminary studies on its potential mechanisms.

**2.8. The Influence of LncRNA AC131009.1 on the Biological Activities of HCC Cells In Vitro.** shRNA was used to knock down AC131009.1 expression, and the AC131009.1 expression levels in HepG2 and HCC-LM3 cells was assessed through qRT-PCR, as shown in Figure 7A. We found an effect of lncRNA AC131009.1 on cell metastasis


https://doi.org/10.1021/acsomega.4c09411
ACS Omega 2024, 9, 49986−49999

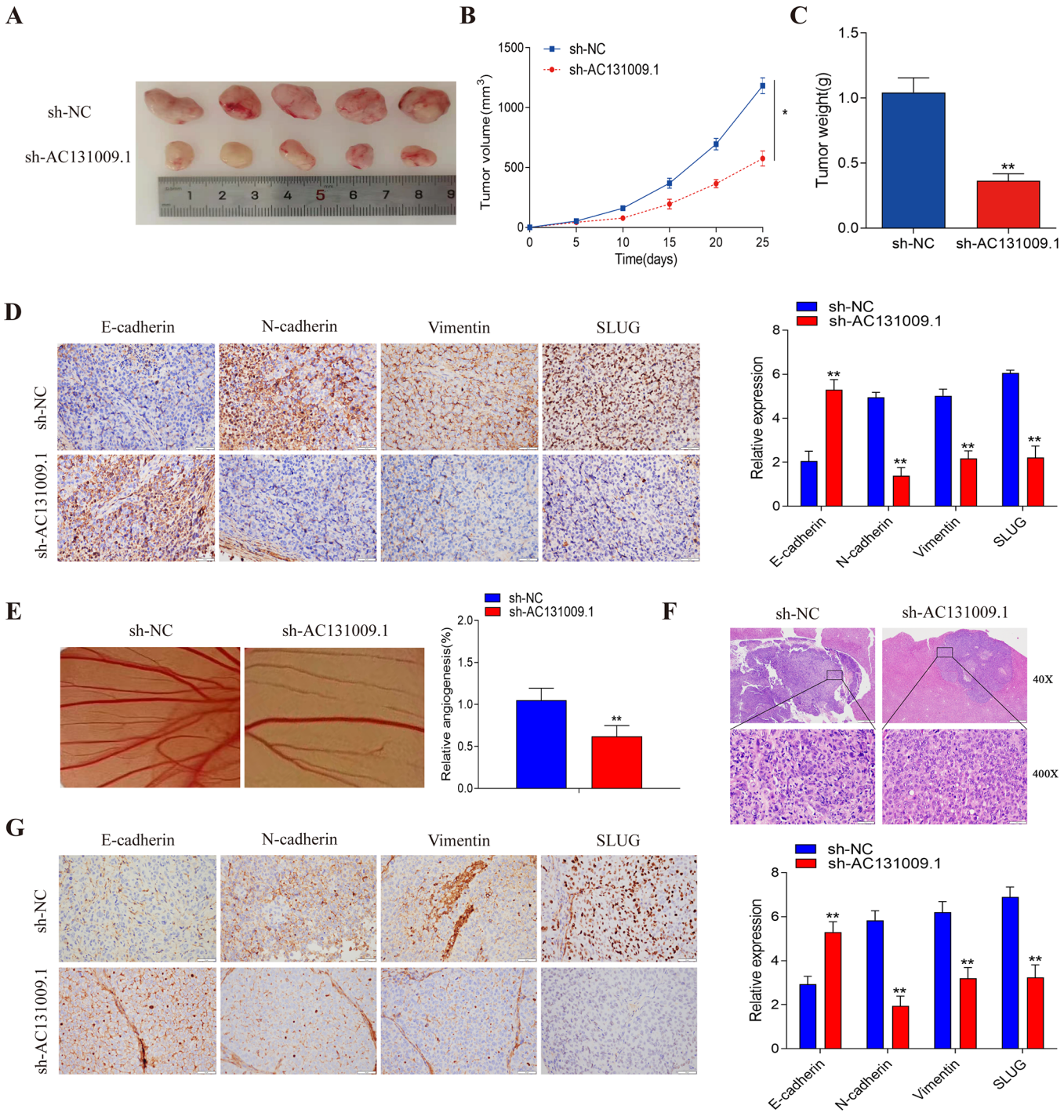


**Figure 8.** Impact of lncRNA AC131009.1 on HCC Cell Proliferation and Metastasis. Tumour dimensions and masses for the sh-AC131009.1 and sh-NC cohorts are depicted in panels A, B, and C. (D) The protein expression levels of E-cadherin, N-cadherin, vimentin and slug were detected in the tumor tissues in each group by IHC. (E) Chicken embryos were exposed to conditioned media (CM) for 4 days, photographed, and their vascular growth was quantified. (F) H&E staining is used to assess the tumor burden in the livers of mice in each group (magnified 40 times and 400 times, respectively). (G) IHC staining is used to measure the expression of E-cadherin, N-cadherin, vimentin, and slug in liver tumors of mice in each group. Data represented as mean ± SD for $n = 5$. Significant difference is indicated by *P < 0.05 and **P < 0.01.

in HCC. As shown in Figure 7B, the knockdown of lncRNA AC131009.1 inhibited the migration of both HCC-LM3 and HepG2 cells in the wound healing assay. Additionally, Transwell assays demonstrated a marked decrease in the migratory and invasive capabilities of cells in the sh-AC131009.1 group relative to the sh-NC control group (Figure 7C).

**2.9. The Silencing of LncRNA AC131009.1 Suppressed the Advancement and Growth of HCC In Vivo.** To investigate the role of AC131009.1 in vivo, male nude mice of 5 weeks old were inoculated with $1 \times 10^7$ HepG2 cells that had been stably transfected (either with shAC131009.1 or sh-NC) into their left flank. The results showed that AC131009.1 knockdown reduced tumor size and



https://doi.org/10.1021/acsomega.4c09411
ACS Omega 2024, 9, 49986−49999

weight (Figure 8A-C). Moreover, the effect of AC131009.1 on EMT-related markers was also detected by Immunohistochemistry (IHC). In the group with reduced AC131009.1 expression, there was an upregulation of the epithelial marker E-cadherin, whereas in the sh-NC group, markers associated with mesenchymal cells (N-cadherin, vimentin, and slug) were more prominently expressed (Figure 8D). Then, the CAM experiment was used to further examine the effect of AC131009.1 on HCC angiogenesis, and the number of new blood vessel formations in the sh-AC131009.1 group was markedly diminished in contrast to the control group (Figure 8E).

To further validate our findings, we conducted an orthotopic HCC model experiment. HE staining of the orthotopic HCC tissues revealed that, at 40× magnification, the HCC in the sh-NC control group were noticeably larger compared to those in the sh-AC131009.1 group. At 400× magnification, tumor cells in the sh-NC group displayed irregular, spindle-shaped morphology with significant pleomorphism, alongside characteristics indicative of stromal transformation. In contrast, tumor cells in the sh-AC131009.1 group exhibited relatively regular morphology with reduced pleomorphism compared to the control group (Figure 8F). Additionally, IHC staining analysis revealed an increase in the expression of the epithelial marker E-cadherin in the sh-AC131009.1 group, while mesenchymal markers such as N-cadherin, vimentin, and slug were expressed at higher levels in the sh-NC group (Figure 8G). Collectively, these findings suggest that the knockdown of AC131009.1 inhibits the proliferation and metastatic potential of HCC cells, leading to a decreased capacity for EMT.

## 3. MATERIALS AND METHODS

**3.1. Data Sources.** RNA sequencing data for HCC patients were acquired from the TCGA-LIHC data set, accessible via the GDC portal (https://portal.gdc.cancer.gov/). Complementary clinical information was sourced through the cBioPortal platform (http://www.cbioportal.org/). Study participants met predefined inclusion criteria: (1) clear classification of VI status in HCC specimens and (2) availability of complete RNA-Seq data for both lncRNAs and mRNA. Patients with a survival period of 0 or missing survival information were excluded. Ultimately, this study included 106 HCC patients with VI and 206 HCC patients without VI. Ten disulfidptosis-related genes, namely, SLC7A11,GYS1, RPN1, OXSM, LRPPRC, NUBPL, NCKAP1, NDUFS1, SLC3A2, and NDUFA11, were identified from prior research. The association between lncRNAs and the expression levels of these ten genes related to disulfidptosis was calculated using the wilcox.test() function in R software for rank analysis. DRLRs were identified according to the standards of having a correlation coefficient greater than 0.4 and a p-value of less than 0.001. Given that patient data were extracted from the TCGA database, compliance with TCGA's publication guidelines was ensured, eliminating the necessity for ethical clearance.

**3.2. Development and Verification of a Predictive Risk Assessment Model.** First, a univariate Cox regression analysis was conducted to identify DRLRs that exhibit a significant correlation with OS in HCC patients with vascular invasion (VI+) ($P < 0.05$). The selection of pertinent DRLRs was further refined employing the LASSO regression analysis to control for overfitting in the modeling process effectively. Subsequently, a multivariate Cox regression analysis was conducted to establish the optimal prognostic risk model using the DRLRs with the lowest akaike information criterion (AIC) value. The risk score for each VI+ HCC patient was computed with the following equation: Risk score = (Expression level of lncRNA A * Coefficient of lncRNA A) + (Expression level of lncRNA B * Coefficient of lncRNA B) + ... To validate the prognostic model, we created a new internal validation cohort comprising 106 VI+ HCC patients, using the bootstrap resampling technique, which is strongly advocated for the internal validation of prognostic models.[20−22] Subsequently, the participants in the training cohort were classified into low-risk and high-risk categories based on their median risk scores. Kaplan−Meier survival curves were generated using the 'Survival' and 'Survminer' R packages, while time-dependent ROC (timeROC) curves were plotted with the 'timeROC' package to assess the prediction model's effectiveness. Multiple ROC analyses were executed to contrast the prognostic utility of the risk model against individual clinical variables. The model's predictive accuracy was evaluated through C-index analysis using R packages like 'dplyr', 'rms', and 'pec'. Risk score distribution for DRLRs, survival status of each patient, and the expression risk heatmap corresponding to each DRLR in the samples were constructed using the pheatmap package. Finally, three-dimensional PCA plots were created via the R packages limma and scatterplot3d to visualize the differentiation value of all genes, disulfidptosis-related mRNA, DRLRs, and the prognostic signature model in distinguishing among VI+ HCC patients classified into low-risk and high-risk categories.

**3.3. Construction of a Prognosis Nomogram.** To assess the prognostic significance of the risk model in combination with clinical characteristics and to determine its independent prognostic value for patients with VI+ HCC, both univariate and multivariate Cox regression analyses were performed. The R package 'rms' was employed to develop a nomogram for predicting OS at 1, 3, and 5 years in patients with VI+ HCC. The predictive accuracy of this nomogram was assessed using calibration curves.

**3.4. Analysis of Pathway Enrichment and Gene Set Enrichment.** Differential expression evaluation to determine significantly DEGs between low-risk and high-risk cohort, as defined by the risk model, was performed using the 'limma' package in R. Genes were selected based on a log2 fold change exceeding 1 and an FDR below 0.05. These DEGs underwent functional enrichment analysis leveraging the GO database, which provides annotations and classifications for genes according to biological processes (BP), molecular functions (MF), and cellular components (CC). Furthermore, GSEA was performed to identify crucial biological functions and pathways significantly linked with VI+ HCC in both risk groups. GSEA employed three gene sets, namely, c5.all.v2022.1.Hs.symbols.gmt, c2.all.v2022.1.Hs.symbols.gmt, and h.all.v2022.1.Hs.symbols.gmt, considering terms significantly enriched with a P value and FDR both under 0.05. The R packages'org.Hs.eg.db', 'clusterProfiler',and 'enrichplot' facilitated the aforementioned enrichment analyses.

**3.5. Immunity Landscape Assessment.** The CIBERSORT methodology was employed to estimate the proportions of immune cells infiltrating tumors within every specimen from VI+ HCC patients. Postanalysis, results were filtered using a statistical significance threshold of $P < 0.05$. To analyze differences in immune cell quantities and functions, the ssgsea computational method was utilized alongside R packages such


https://doi.org/10.1021/acsomega.4c09411
ACS Omega 2024, 9, 49986−49999

as limma, reshape2, ggpubr, GSVA, and GSEABase. Box plots were generated to depict the proportions of immune cells in VI + HCC samples, facilitating a comparative evaluation of immune cell content and function between groups at varying risks.

**3.6. Selecting Suitable Drugs for VI+ HCC Patients via OncoPredict.** Maeser et al.[23] developed an R package called oncopredict to predict drug responses in tumor patients. First, the oncopredict package was utilized to evaluate the drug sensitivity scores for each sample. Subsequently, the ggpubr and limma packages were employed to predict the variation in drug responsiveness between the low-risk and high-risk cohorts. The filtering criterion was set at $P < 0.05$. A reduced half maximal inhibitory concentration (IC50) value signifies greater sensitivity to the drug, which can guide the clinical selection of drugs for patients.

**3.7. Bioinformatic Assessment of Prognostic hub DRLRs in the Model.** The hub DRLRs integral to the risk prognosis model underwent an exhaustive bioinformatics scrutiny. Wilcox tests were conducted on these DRLRs with R packages ggpubr, plyr, and reshape2 to ascertain pancancer variances between tumor tissues and adjacent normal tissues across 32 cancer types within the TCGA database. Pearson correlation analysis identified mRNA genes that are significantly correlated with prognosis DRLRs. applying a filtering criterion of correlation coefficient exceeding 0.4 along with a p-value below 0.001. The visualization of results was achieved using the R package ComplexHeatmap. GO analysis was executed on genes that are coexpressed with the hub DRLRs. Additionally, all sample was grouped according to hub DRLR expression (high vs low based on the median expression level). This was followed by GSEA. Furthermore, an assessment of drug sensitivity and an analysis of immune cell infiltration were performed for each distinct hub DRLR.

**3.8. Cell Culture and Transfection.** HCC cell lines, namely HCC-LM3, Hep3B2.1−7, and HepG2, along with the L02 cell line, were procured from the Cell Bank of the Chinese Academy of Medical Sciences located in Shanghai, China. These cells were cultured using DMEM, which was supplemented with 10% fetal bovine serum (FBS, Gibco), as well as 100 U/mL penicillin (Gibco) and 100 $\mu$g/mL streptomycin, maintaining an environment of 37 °C in 5% CO2. GenePharma constructed the shRNA targeted against AC131009.1 (sh-AC131009.1) and a negative control shRNA (sh-NC). Cell transfections were performed utilizing Lipofectamine 3000 (Invitrogen) reagent.

**3.9. QRT-PCR to Determine Prognostic Hub DRLRs Expression in Different HCC Cell Lines in the Model.** Expression levels of pivotal prognostic DRLRs were assessed across various HCC cell lines, such as Hep3B2.1−7, HepG2, and HCC-LM3. The L02 cell line was employed as a normal control for comparison purposes. These cell lines were procured from the Chinese Academy of Sciences Cell Bank situated in Shanghai. Total RNA extraction was conducted using TRIzol reagent as per the manufacturer's instructions, followed by cDNA synthesis. Subsequently, we conducted experiments using qRT-PCR technology with cDNA as the template. GAPDH, the human housekeeping gene, was selected as the internal control for normalizing relative expression levels, using the $2-\Delta\Delta Ct$ method. Detailed primer sequences can be found in Table S2.

**3.10. Wound Healing Assay.** Various groups of HCC cells were cultured in six-well plates to achieve over 90% confluence, at which point a scratch was made across the center of each well using a pipet tip. The cells were then washed twice with PBS, and medium devoid of FBS was introduced into each well. Photographs were captured using an inverted microscope, measuring the mean gap width with a caliper. After 48 h, additional images were taken to assess changes.

**3.11. Cell Migration and Invasion Assays.** For the Transwell analysis, HCC cells were introduced into Transwell chambers, which were either covered with Matrigel Basement Membrane (BD Biosciences) or left uncoated. A total of $4 \times 10^4$ HCC cells suspended in 200 $\mu$L of serum-free medium were placed in the upper chamber of the Transwell. A suspension comprising 40,000 HCC cells in 200 $\mu$L of medium devoid of serum was introduced into the upper compartment of the Transwell setup. For the invasion assay, Matrigel was applied to the upper chamber in a 50 $\mu$L coating. After incubation for 24 h in 5% CO2 at 37 °C, the cells were preserved with 4% paraformaldehyde and subsequently stained with 0.1% crystal violet. Observations and imaging were conducted by selecting five random fields under an inverted microscope.

**3.12. A Model Using the Chorioallantoic Membrane (CAM) of Chick Embryos.** Fresh fertilized White Laihang chicken eggs were sourced from Shanghai Huguang Poultry Breeding Co., Ltd. After disinfecting the eggs with 70% ethanol, they were cultured at 37 °C and 65% humidity, marking embryo development day 1 (EDD-1). A minor aperture was created on EDD-3 on the egg's apex and sealed with cellophane to prevent dehydration and contamination, and incubation proceeded with the eggs in a static, upright position until EDD-10. At EDD-10, the embryos' viability and the vascular system of CAM are visually examined before addition processing.[24] Intra egg studies adhered to ethical constraints, not extending beyond EDD-17.[25] The stable transfected HCC-LM3 cell suspension (sh-AC131009.1 or sh-NC) was mixed with growth factor reduced Matrigel (1:1). Then load the mixture onto the top of CAM at a density of 5 × 105 cells per embryo. After implantation, the eggs were protected with tape and then returned to the incubator. The eggs were observed daily after transplantation until EDD-14. On EDD-14, macroscopic observation of vascular growth was conducted using a stereomicroscope, and the angiogenic effect was quantified by calculating the number of vascular branches for each ovum.

**3.13. Tumour Formation In Vivo.** Specific pathogen-free (SPF) grade male BALB/c nude mice, aged 5 weeks, procured from Shanghai SLAC Laboratory Animal Co. Ltd., were randomly assigned into experimental groups. Each mouse was inoculated at the left flank with $1 \times 10^7$ stable transfected HepG2 cells (sh-AC131009.1 or sh-NC). Tumor volume (V) evaluations were conducted every 5 days, calculated using the formula: $V = \text{length} \times \text{width}^2/2$. Twenty-5 days post-inoculation, the mice were euthanized, and subcutaneous tumors were excised and imaged. Then, the weight of the tumor tissues was detected. Subsequently, the tumor tissues were stored in liquid nitrogen for subsequent experiments. Handling was performed in accordance with the guidelines outlined in the "Guide for the Care and Use of Laboratory Animals" by the National Institutes of Health. All animal experimental work received approval (JRSRMYY-2023−042) from the Medical Ethics Committee of Jurong Hospital Affiliated to Jiangsu University. All the experiments were


https://doi.org/10.1021/acsomega.4c09411
ACS Omega 2024, 9, 49986−49999

performed in accordance with all national or local guidelines and regulations.

**3.14. The Orthotopic HCC Model Induced by HCC-LM3 Cells in Nude Mice.** We employed BALB/c nude mice of SPF grade, obtained from the Shanghai SLAC Laboratory Animal Co. Ltd. (Shanghai, China). The allocation of these mice into two groups was performed in a random manner. HCC-LM3 cells (either sh-AC131009.1 or sh-NC) were expanded in culture. When the HCC cells reached 70% to 80% confluence, they were subcultured at a 1:3 ratio into three 75 $cm^2$ culture flasks and supplemented with an appropriate volume of culture medium to maintain optimal cell conditions. Upon reaching the logarithmic phase of growth, the cells were collected for the purpose of inoculation. Six-week-old male nude mice were inoculated with 1 × 106 of these stably transfected HCC-LM3 cells (either sh-AC131009.1 or sh-NC) directly into the capsule of the left liver lobe. After 8 weeks, the nude mice were euthanized, and their liver and lung tissues were removed. Subsequently, the tumor tissues were stored in liquid nitrogen for subsequent experiments.

**3.15. Immunohistochemistry.** To elucidate the role of AC131009.1 in HCC cell proliferation and invasion, alongside epithelial-mesenchymal transition (EMT) involvement, tissue obtained from mice underwent fixation in 4% paraformaldehyde for 48 h and subsequent sectioning into 5 $\mu$m slices. After sections were initially treated with 5% goat serum to block nonspecific binding, they were subsequently incubated with primary antibodies: E-cadherin (1:500; Abcam), N-cadherin (1:500; Abcam), Vimentin (1:250; Abcam), and Slug (1:100; Cell Signaling). Secondary antibody incubation (1:500; Santa Cruz) was conducted for 2 h at 37 °C. The immunohistochemistry scoring criteria, adopted from previous standards,[26] were as follows: immunostaining intensity was classified into four levels: 0 (negative), 1 (weak), 2 (moderate), and 3 (strong). The staining percentage was classified as follows: 1 (0%∼$10%), 2 (11%∼50%), 3 (51%∼80%), and 4 (81%∼100%), with the intensity and percentage summations providing the final immunohistochemistry score (IHS). Two independent pathologists blindly assessed all immunostained sections.

**3.16. Hematoxylin−Eosin Staining (HE).** Tumor specimens were preserved using a 4% paraformaldehyde solution for a 24-h period, subsequently undergoing dehydration and embedding in paraffin. These samples were then sectioned into continuous slices of 4 $\mu$m thickness. Hematoxylin and eosin (H&E) staining was performed using a kit from Beyotime (Shanghai, China, C0105S). The stained samples were examined under a microscope (OLYMPUS BX53, Tokyo, Japan).

**3.17. Statistics.** In this study, we conducted data processing and graphical plotting using software version 4.1.3 (http://www.R-project) and SPSS statistical software version 19.0 (SPSS Inc., Chicago, IL, USA). statistical significance is established when the p-value falls below the threshold of 0.05.

## 4. DISCUSSION

HCC continues to pose a major worldwide public health challenge, with its precise treatment being significantly impeded by tumor heterogeneity. The capacity of cancer cells to evade physiological cell death mechanisms serves as a fundamental basis for the onset and advancement of malignant disease. Cancer cells are commonly perceived as lacking the ability to undergo self-destruction, a phenomenon closely intertwined with the processes of tumor growth and metastasis.[27] VI has been identified as a prominent risk factor for recurrence in HCC, affecting approximately 25−50% of patients.[28−30] It is an essential prerequisite for tumor growth, as vascular invasion facilitates the dissemination of invasive tumor cells from the primary tumor site and their subsequent metastasis.[31,32] VI can be classified into micro and macro types, both of which are closely linked to tumor recurrence and survival rates.[10,33] In liver transplant recipients, the diagnosis of vascular invasion is crucial in determining the recurrence frequency and OS. Compared to liver transplant patients without vascular invasion, those with vascular invasion experience a 50% higher mortality rate.[34,35] Therefore, the creation of novel predictive models for evaluating the prognosis of VI in HCC patients may provide crucial insights for diagnosis and therapeutic strategies. Recently, a newly identified mechanism of cellular demise, known as disulfidptosis, has emerged. It is triggered by disulfide stress and differs significantly from previously studied forms of programmed cellular demise, including mechanisms like cuproptosis, apoptosis, ferroptosis, necrotic apoptosis, and pyroptosis.[15,36] Disulfidptosis is identified by an excessive intracellular accumulation of disulfide bond molecules and a reduction in NADPH levels.[15] Disulfides also play a critical role as regulators of oxidative metabolism, influencing the survival of tumor cells and the process of tumor metastasis.[37] Research has indicated that abnormal disulfidptosis has profound implications for tumor progression and drug resistance.[38] Undoubtedly, this innovative concept of disulfidptosis as a programmed cell death mechanism will contribute to further exploration and a more comprehensive understanding of cell death mechanisms. It holds the potential to provide a new therapeutic approach for targeting disulfidptosis in cancer treatment.[39,40] LncRNAs have been recognized as potential diagnostic, prognostic, and therapeutic targets for HCC.[21,41,42] Therefore, we believe that DRLRs have significant value in facilitating the understanding of the occurrence and prognostic evaluation of HCC. As of the present moment, the role of DRLRs in HCC, especially regarding the more aggressive VI+ type, remains undocumented. Consequently, our objective was to construct a predictive framework for patients with VI+ HCC predicated on DRLRs and examine the expression profiles of hub DRLRs in VI+ HCC and their correlations with immune cell infiltration, their enrichment in biological pathways, and their value in drug sensitivity analysis. Our research has demonstrated that the expression of AC131009.1 is markedly higher in highly invasive human HCC-LM3 cells than in less invasive human HCC Hep3B2.1−7 cells and in HepG2 cells with low invasion potential. This expression pattern across cell types with different invasive abilities suggests that AC131009.1 may be a crucial lncRNA influencing HCC invasion and metastasis. Consequently, we conducted further studies by suppressing AC131009.1 expression.

We identified lncRNAs associated with VI in HCC patients, distinguishing them from those without VI. We constructed a prognostic model comprising AC009779.2, AC131009.1, and LUCAT1. Cox regression analysis confirmed its independent prognostic value, while Kaplan−Meier survival analysis revealed that individuals classified with elevated risk scores exhibited significantly diminished overall survival rates. Multiple ROC, C-index, and PCA analyses confirmed the precision and efficacy of the model. Additionally, we developed a nomogram for clinical prognosis assessment. The high-risk


https://doi.org/10.1021/acsomega.4c09411
ACS Omega 2024, 9, 49986−49999

patient group primarily participated in various biological pathways related to cell signaling, tumor progression, and cellular immunity. Notably, follicular helper T cells and activated memory T cells were found to be more prevalent in the high-risk group, whereas monocytes were predominantly present in the low-risk cohort. Furthermore, the immunological functionalities of mast cells and B cells were markedly diminished in the high-risk category, while the immune-related activities of MHC class I were enhanced. Sensitivity to pharmacological agents was evaluated, revealing that the high-risk group may demonstrate heightened responsiveness to certain drugs, including AZD4547, BMS-536924, BPD-00008900, dasatinib, and YK-4−279. Conversely, this cohort exhibited a greater propensity to develop resistance to agents such as gemcitabine, irinotecan, mirin, nutlin-3a (−), and PLX-4720.

Among the hallmark hub lncRNAs in our model, LUCAT1 has been identified as an angiogenesis-related lncRNA highly associated with liver cancer prognosis[43] and serves as a prognostic methylation-driven gene.[44] In vitro experiments conducted by Gramantieri et al.[45] revealed that silencing LUCAT1 increased the motility and invasive capabilities of HCC cells, thereby affecting the EMT phenotype. Limited research has been conducted on AC009779.2 and AC131009.1. AC009779.2 has been confirmed as a metabolism-related lncRNA closely linked to the development and clinical outcomes of osteosarcoma.[46] Conversely, AC131009.1 is considered a lncRNA linked to lactate metabolism[47] and necroptosis.[48] However, the specific role and oncogenic mechanisms of AC131009.1 in HCC remain unknown. In our bioinformatics analysis of lncRNA AC131009.1, we observed differential expression in various tumors and enrichment in biological pathways related to tumor development, immunity, and the response to multiple metal ions. AC131009.1 exhibited correlations with different types of immune cells, displaying a notable positive association with M0 macrophages and a marked inverse relationship with monocytes and activated NK cells. displaying a significant positive correlation with M0 macrophages and a significant negative correlation with monocytes and activated NK cells. The group with high expression of AC131009.1 demonstrated greater sensitivity to drugs such as BDP-00009066, BPD-00008900, docetaxel, GDC0810, and ipatasertib. Moreover, knockdown of AC131009.1 and subsequent experiments revealed changes in the motility and invasion of HCC cells, as demonstrated by scratch and Transwell assays. Concurrently, the CAM assay confirmed that the suppression of AC131009.1 reduces the impact of HCC cells on the proliferation and movement of vascular endothelial cells. Additionally, a nude mouse xenograft model and an in vivo orthotopic HCC model were established, and preliminary findings from HE staining and IHC staining of the xenografts indicated a correlation between AC131009.1 and EMT, thus validating its role in promoting EMT in HCC cells. EMT serves as an essential cellular mechanism in tumor progression, contributing to the increased tumorigenicity and metastatic potential of cancer cells.[49] Dysregulated expression of various biomarkers in HCC patients is closely associated with VI. Targeting these biomarkers has the potential to impact HCC cell invasion, metastasis, and EMT through the regulation of intricate mechanisms, making them promising targets for intervention in HCC.[50] Further research is warranted to investigate the specific processes through which disulfidptosis-related AC131009.1 promotes HCC invasion and metastasis through EMT, which could potentially enable targeted therapy for VI+ HCC by specifically targeting disulfidptosis-related AC131009.1.

While this study advances our understanding of the link between lncRNA AC131009.1 and HCC, further mechanistic exploration of its role in cancer progression remains in its infancy. There are certain limitations to our study, including discrepancies among databases, a restricted number of clinical samples, and the retrospective design of sample collection, all of which underscore the necessity for prospective studies to assess and validate the clinical applicability of our model. Moreover, additional molecular studies are essential to verify our results and elucidate the mechanisms through which disulfidptosis-related lncRNA AC131009.1 enhances invasion and metastasis via EMT in HCC.

## 5. CONCLUSIONS

In conclusion, this is the first study analyzing differentially regulated disulfidptosis-related long noncoding RNAs associated with vascular invasion in HCC. We developed and validated a risk model for vascular invasion in HCC patients, distinguishing them from those without vascular invasion. Additionally, we have preliminary evidence suggesting that downregulation of lncRNA AC131009.1 expression restricts the migratory and invasive capabilities of HCC cells, potentially exerting a malignant biological effect through EMT to promote HCC cell invasion and metastasis. Based on this research model, personalized immunotherapy response prediction and treatment selection may be possible for HCC patients. LncRNA AC131009.1 holds promise as a novel target for therapeutic intervention in patients exhibiting vascular invasion in HCC.

## ■ ASSOCIATED CONTENT

### Data Availability Statement

The data supporting this study's findings are mentioned within the manuscript in the results and discussion section. No other data were generated beyond what is provided in this manuscript. Publicly available data sets were analyzed in this study. These data can be found here: https://portal.gdc.cancer.gov/, and https://www.cbioportal.org/. The data sets used and analyzed during the current study are available from the corresponding author upon reasonable request.

### Supporting Information

The Supporting Information is available free of charge at https://pubs.acs.org/doi/10.1021/acsomega.4c09411.

Gene Ontology (GO) analysis and GSEA for AC009779.2 (Figure S1); GO analysis and GSEA for AC131009.1 (Figure S2); GO analysis and GSEA for LUCAT1 (Figure S3); drug sensitivity in VI+ HCC patients with high and low expression of AC009779.2 (Figure S4); drug sensitivity in VI+ HCC patients with high and low expression of AC131009.1 (Figure S5); drug sensitivity in VI+ HCC patients with high and low expression of LUCAT1 (Figure S6); features of vascular HCC patients in the training cohort and the validation cohort (Table S1); and qRT-PCR primer sequences used in this study (Table S2) (PDF)



https://doi.org/10.1021/acsomega.4c09411
ACS Omega 2024, 9, 49986−49999

## AUTHOR INFORMATION


### Corresponding Author

**Jin Huang** − *Department of Gastroenterology, The Affiliated Changzhou Second People's Hospital of Nanjing Medical University, Changzhou, Jiangsu 213003, China;* orcid.org/0009-0002-0787-3915; Phone: +86- 0519-88104931; Email: hj042153@163.com; Fax: +86- 0519-88104931

### Authors

**Xuefeng Gu** − *Department of Infectious Diseases, Jurong Hospital Affiliated to Jiangsu University, Zhenjiang, Jiangsu 212400, China;* orcid.org/0000-0002-6198-2568

**Yanyan Wei** − *Department of Infectious Diseases, The First Affiliated Hospital of Anhui Medical University, Hefei, Anhui 230022, China;* orcid.org/0000-0001-7925-7500

**Mao Lu** − *Department of Gastroenterology, The Affiliated Changzhou Second People's Hospital of Nanjing Medical University, Changzhou, Jiangsu 213003, China*

**Duo Shen** − *Department of Gastroenterology, The Affiliated Changzhou Second People's Hospital of Nanjing Medical University, Changzhou, Jiangsu 213003, China;* orcid.org/0000-0002-2715-1090

**Xin Wu** − *Department of General Surgery, The Fourth Affiliated Hospital of Nanjing Medical University, Nanjing, Jiangsu 210000, China*

Complete contact information is available at: https://pubs.acs.org/10.1021/acsomega.4c09411


### Author Contributions

J.H., D.S., and X.W. designed the study; X.F.G. collected data and prepared figures and tables; X.F.G., D.S., Y.Y.W., and M.L. performed the experiments and data analyses; Y.Y.W. provided funding; X.F.G. drafted the manuscript; J.H., D.S., and X.W. supervised the study. All authors read and approved the final manuscript.


### Funding

This study was supported by the Natural Science Foundation of Anhui Province (project 2108085QH312), the Basic and Clinical Cooperative Research Promotion Plan of Anhui Medical University (project 2022xkjT003), and the Anhui Medical University Doctoral Research Foundation (project BSKY2019034).


### Notes

The authors declare no competing financial interest.

## ACKNOWLEDGMENTS

We express our sincere gratitude to Dr. Chuanbing Shi from the Nanjing Pukou People's Hospital, Pukou Branch of Jiangsu Province Hospital, and Dr. Zhe Zhang from the Jiangsu Cancer Hospital, Affiliated Cancer Hospital of Nanjing Medical University, for their meticulous assessment of the IHC results.

## REFERENCES


(1) Sung, H.; Ferlay, J.; Siegel, R. L.; Laversanne, M.; Soerjomataram, I.; Jemal, A.; Bray, F. Global cancer statistics 2020: GLOBOCAN estimates of incidence and mortality worldwide for 36 cancers in 185 countries. *CA Cancer J. Clin.* **2021**, *71*, 209−49.

(2) Llovet, J. M.; Kelley, R. K.; Villanueva, A.; Singal, A. G.; Pikarsky, E.; Roayaie, S.; Lencioni, R.; Koike, K.; Zucman-Rossi, J.; Finn, R. S. Hepatocellular carcinoma. *Nat. Rev. Dis Primers.* **2021**, *7*, 6.

(3) Yang, Y. Q.; Wen, Z. Y.; Liu, X. Y.; Ma, Z. H.; Liu, Y. E.; Cao, X. Y.; Hou, L.; Xie, H. Current status and prospect of treatments for recurrent hepatocellular carcinoma. *World J. Hepatol.* **2023**, *15*, 129−150.

(4) Sangro, B.; Sarobe, P.; Hervás-Stubbs, S.; Melero, I. Advances in immunotherapy for hepatocellular carcinoma. *Nat. Rev. Gastroenterol. Hepatol.* **2021**, *18*, 525−543.

(5) Zongyi, Y.; Xiaowu, L. Immunotherapy for hepatocellular carcinoma. *Cancer Lett.* **2020**, *470*, 8−17.

(6) Huang, A.; Yang, X. R.; Chung, W. Y.; Dennison, A. R.; Zhou, J. Targeted therapy for hepatocellular carcinoma. *Signal Transduct Target Ther.* **2020**, *5*, 146.

(7) He, Y.; Lu, M.; Che, J.; Chu, Q.; Zhang, P.; Chen, Y. Biomarkers and future perspectives for hepatocellular carcinoma immunotherapy. *Front Oncol.* **2021**, *11*, No. 716844.

(8) Siegel, R. L.; Miller, K. D.; Fuchs, H. E.; Jemal, A. Cancer statistics, 2022. *CA Cancer J. Clin.* **2022**, *72*, 7−33.

(9) Lo, Y. C.; Hsu, F. C.; Hung, S. K.; Tseng, K. C.; Hsieh, Y. H.; Lee, M. S.; Tseng, C. W.; Lin, H. Y.; Chen, L. C.; Chiou, W. Y. Prognosticators of hepatocellular carcinoma with intrahepatic vascular invasion. *Tzu Chi Med. J.* **2019**, *31*, 40−46.

(10) Hsieh, C. H.; Wei, C. K.; Yin, W. Y.; Chang, C. M.; Tsai, S. J.; Wang, L. Y.; Chiou, W. Y.; Lee, M. S.; Lin, H. Y.; Hung, S. K. Vascular invasion affects survival in early hepatocellular carcinoma. *Mol. Clin Oncol.* **2015**, *3*, 252−6.

(11) Erstad, D. J.; Tanabe, K. K. Prognostic and therapeutic implications of microvascular invasion in hepatocellular carcinoma. *Ann. Surg Oncol.* **2019**, *26*, 1474−93.

(12) Zeng, S.; Wang, Z.; Zhu, Q.; Li, X.; Ren, H.; Qian, B.; Hu, F.; Xu, L.; Zhai, B. Identification of risk and prognostic factors for intrahepatic vascular invasion in patients with hepatocellular carcinoma: a population-based study. *Transl Cancer Res.* **2023**, *12*, 93−112.

(13) Peng, J.; Zhang, J.; Zhang, Q.; Xu, Y.; Zhou, J.; Liu, L. A radiomics nomogram for preoperative prediction of microvascular invasion risk in hepatitis B virus-related hepatocellular carcinoma. *Diagn Interv Radiol.* **2018**, *24*, 121−7.

(14) Wang, K.; Xiang, Y.; Yan, J.; Zhu, Y.; Chen, H.; Yu, H.; Cheng, Y.; Li, X.; Dong, W.; Ji, Y.; et al. A deep learning model with incorporation of microvascular invasion area as a factor in predicting prognosis of hepatocellular carcinoma after R0 hepatectomy. *Hepatol Int.* **2022**, *16*, 1188−98.

(15) Liu, X.; Nie, L.; Zhang, Y.; Yan, Y.; Wang, C.; Colic, M.; Olszewski, K.; Horbath, A.; Chen, X.; Lei, G.; et al. Actin cytoskeleton vulnerability to disulfide stress mediates disulfidptosis. *Nat. Cell Biol.* **2023**, *25*, 404−14.

(16) Mattick, J. S.; Amaral, P. P.; Carninci, P.; Carpenter, S.; Chang, H. Y.; Chen, L. L.; Chen, R.; Dean, C.; Dinger, M. E.; Fitzgerald, K. A.; et al. Long non-coding RNAs: definitions, functions, challenges and recommendations. *Nat. Rev. Mol. Cell Biol.* **2023**, *24*, 430−47.

(17) Peng, W.; Bai, S.; Zheng, M.; Chen, W.; Li, Y.; Yang, Y.; Zhao, Y.; Xiong, S.; Wang, R.; Cheng, B. An exosome-related lncRNA signature correlates with prognosis, immune microenvironment, and therapeutic responses in hepatocellular carcinoma. *Transl Oncol.* **2023**, *31*, No. 101651.

(18) Guo, D. F.; Fan, L. W.; Zeng, H. H.; Huang, C. B.; Wu, X. H. Establishment and validation of a cuproptosis-related lncRNA signature that predicts prognosis and potential targeted therapy in hepatocellular carcinoma. *Biotechnol. Genet. Eng. Rev.* **2023**, *40*, 739−764.

(19) Wang, W.; Ye, Y.; Zhang, X.; Sun, W.; Bao, L. An angiogenesis-related three-long non-coding ribonucleic acid signature predicts the immune landscape and prognosis in hepatocellular carcinoma. *Heliyon.* **2023**, *9*, No. e13989.

(20) Blackstone, E. H. Breaking down barriers: helpful breakthrough statistical methods you need to understand better. *J. Thorac Cardiovasc Surg.* **2001**, *122*, 430−9.

(21) Gu, X.; Li, H.; Sha, L.; Zhao, W. A prognostic model composed of four long noncoding RNAs predicts the overall survival of Asian patients with hepatocellular carcinoma. *Cancer Med.* **2020**, *9*, 5719−30.

(22) Gu, X.; Sha, L.; Zhang, S.; Shen, D.; Zhao, W.; Yi, Y. Neutrophils and lymphocytes can help distinguish asymptomatic COVID-19 from moderate COVID-19. *Front Cell Infect Microbiol.* **2021**, *11*, No. 654272.
(23) Maeser, D.; Gruener, R. F.; Huang, R. S. OncoPredict: an R package for predicting in vivo or cancer patient drug response and biomarkers from cell line screening data. *Brief Bioinform.* **2021**, *22*, bbab260.
(24) Kue, C. S.; Tan, K. Y.; Lam, M. L.; Lee, H. B. Chick ∼ embryo ∼ chorioallantoic ∼ membrane∼(CAM): an ∼ alternative ∼ predictive ∼ model ∼ in acute toxicological studies for anti-cancer drugs. *Exp Anim.* **2015**, *64*, 129−38.
(25) Khabib, M. N. H.; Sivasanku, Y.; Lee, H. B.; Kumar, S.; Kue, C. S. Alternative animal models in predictive toxicology. *Toxicology.* **2022**, *465*, No. 153053.
(26) Gu, X.; Fu, M.; Ge, Z.; Zhan, F.; Ding, Y.; Ni, H.; Zhang, W.; Zhu, Y.; Tang, X.; Xiong, L.; et al. High expression of MAGE-A9 correlates with unfavorable survival in hepatocellular carcinoma. *Sci. Rep.* **2014**, *4*, 6625.
(27) Zhao, Y.; Zhang, Y. N.; Wang, K. T.; Chen, L. Lenvatinib for hepatocellular carcinoma: from preclinical mechanisms to anti-cancer therapy. *Biochim Biophys Acta Rev. Cancer.* **2020**, *1874*, No. 188391.
(28) Lee, Y. H.; Hsu, C. Y.; Huang, Y. H.; Hsia, C. Y.; Chiou, Y. Y.; Su, C. W.; Lin, H. C.; Huo, T. I. Vascular invasion in hepatocellular carcinoma: prevalence, determinants and prognostic impact. *J. Clin Gastroenterol.* **2014**, *48*, 734−41.
(29) Kurokawa, T.; Yamazaki, S.; Mitsuka, Y.; Moriguchi, M.; Sugitani, M.; Takayama, T. Prediction of vascular invasion in hepatocellular carcinoma by next-generation des-r-carboxy prothrombin. *Br J. Cancer.* **2016**, *114*, 53−8.
(30) Gouw, A. S. H.; Balabaud, C.; Kusano, H.; Todo, S.; Ichida, T.; Kojiro, M. Markers for microvascular invasion in hepatocellular carcinoma: where do we stand? *Liver Transplant.* **2011**, *17* (S2), S72−S80.
(31) Mittal, K.; Ebos, J.; Rini, B. Angiogenesis and the tumor microenvironment: vascular endothelial growth factor and beyond. *Semin Oncol.* **2014**, *41*, 235−51.
(32) Zhang, R.; Ye, J.; Huang, H.; Du, X. Mining featured biomarkers associated with vascular invasion in HCC by bioinformatics analysis with TCGA RNA sequencing data. *Biomed Pharmacother.* **2019**, *118*, No. 109274.
(33) Sumie, S.; Nakashima, O.; Okuda, K.; Kuromatsu, R.; Kawaguchi, A.; Nakano, M.; Satani, M.; Yamada, S.; Okamura, S.; Hori, M.; et al. The significance of classifying microvascular invasion in patients with hepatocellular carcinoma. *Ann. Surg Oncol.* **2014**, *21*, 1002−9.
(34) Mazzaferro, V.; Llovet, J. M.; Miceli, R.; Bhoori, S.; Schiavo, M.; Mariani, L.; Camerini, T.; Roayaie, S.; Schwartz, M. E.; Grazi, G. L.; et al. Predicting survival after liver transplantation in patients with hepatocellular carcinoma beyond the Milan criteria: a retrospective, exploratory analysis. *Lancet Oncol.* **2009**, *10*, 35−43.
(35) Filgueira, N. A. Hepatocellular carcinoma recurrence after liver transplantation: risk factors, screening and clinical presentation. *World J. Hepatol.* **2019**, *11*, 261−72.
(36) Machesky, L. M. Deadly actin collapse by disulfidptosis. *Nat. Cell Biol.* **2023**, *25*, 375−6.
(37) Min, H. Y.; Lee, H. Y. Oncogene-driven metabolic alterations in cancer. *Biomol Ther (Seoul).* **2018**, *26*, 45−56.
(38) Zheng, P.; Zhou, C.; Ding, Y.; Duan, S. Disulfidptosis: a new target for metabolic cancer therapy. *J. Exp Clin Cancer Res.* **2023**, *42*, 103.
(39) Hadian, K.; Stockwell, B. R. The therapeutic potential of targeting regulated non-apoptotic cell death. *Nat. Rev. Drug Discovery* **2023**, *22*, 723−42.
(40) Liu, X.; Zhuang, L.; Gan, B. Disulfidptosis: disulfide stress-induced cell death. *Trends Cell Biol.* **2024**, *34*, 327.
(41) Hou, Y. R.; Diao, L. T.; Hu, Y. X.; Zhang, Q. Q.; Lv, G.; Tao, S.; Xu, W. Y.; Xie, S. J.; Zhang, Q.; Xiao, Z. D. The conserved LncRNA DIO3OS restricts hepatocellular carcinoma stemness by interfering with NONO-mediated nuclear export of ZEB1 mRNA. *Adv. Sci. (Weinh).* **2023**, *10*, No. e2301983.
(42) Peng, J. Y.; Cai, D. K.; Zeng, R. L.; Zhang, C. Y.; Li, G. C.; Chen, S. F.; Yuan, X. Q.; Peng, L. Upregulation of superenhancer-driven LncRNA FASRL by USF1 promotes de novo fatty acid biosynthesis to exacerbate hepatocellular carcinoma. *Adv. Sci. (Weinh).* **2023**, *10*, No. e2204711.
(43) Xie, S.; Zhong, J.; Zhang, Z.; Huang, W.; Lin, X.; Pan, Y.; Kong, X.; Xia, H.; Yu, Z.; Ni, H.; et al. Novel risk model based on angiogenesis-related lncRNAs for prognosis prediction of hepatocellular carcinoma. *Cancer Cell Int.* **2023**, *23*, 159.
(44) Fu, J.; Qin, W.; Tong, Q.; Li, Z.; Shao, Y.; Liu, Z.; Liu, C.; Wang, Z.; Xu, X. A novel DNA methylation-driver gene signature for long-term survival prediction of hepatitis-positive hepatocellular carcinoma patients. *Cancer Med.* **2022**, *11*, 4721−35.
(45) Gramantieri, L.; Baglioni, M.; Fornari, F.; Laginestra, M. A.; Ferracin, M.; Indio, V.; Ravaioli, M.; Cescon, M.; De Pace, V.; Leoni, S.; et al. LncRNAs as novel players in hepatocellular carcinoma recurrence. *Oncotarget.* **2018**, *9*, 35085−99.
(46) Chen, X.; Ye, Z.; Lou, P.; Liu, W.; Liu, Y. Comprehensive analysis of metabolism-related lncRNAs related to the progression and prognosis in osteosarcoma from TCGA. *J. Orthop Surg Res.* **2021**, *16*, 523.
(47) Guan, Q.; Pan, J.; Ren, N.; Qiao, C.; Wei, M.; Li, Z. Identification of novel lactate metabolism signatures and molecular subtypes for prognosis in hepatocellular carcinoma. *Front Cell Dev Biol.* **2022**, *10*, No. 960277.
(48) Wang, W.; Ye, Y.; Zhang, X.; Ye, X.; Liu, C.; Bao, L. Construction of a necroptosis-associated long non-coding RNA signature to predict prognosis and immune response in hepatocellular carcinoma. *Front Mol. Biosci.* **2022**, *9*, No. 937979.
(49) Dongre, A.; Weinberg, R. A. New insights into the mechanisms of epithelial-mesenchymal transition and implications for cancer. *Nat. Rev. Mol. Cell Biol.* **2019**, *20*, 69−84.
(50) Zhao, X.; Wang, Y.; Xia, H.; Liu, S.; Huang, Z.; He, R.; Yu, L.; Meng, N.; Wang, H.; You, J.; et al. Roles and molecular mechanisms of biomarkers in hepatocellular carcinoma with microvascular invasion: a review. *J. Clin. Transl. Hepatol.* **2023**, *11*, 1170−1183.


https://doi.org/10.1021/acsomega.4c09411
*ACS Omega* 2024, 9, 49986−49999